AIP Journal of Applied Physics

Electric-field-induced dielectric anomalies and optical birefringence in Pb (Zn 1/3 Nb 2/3) 1 − x Ti x O 3 (x = 0.10) single crystal

C.-S. Tu, F.-T. Wang, R. R. Chien, V. H. Schmidt, and L.-C. Lim

Citation: Journal of Applied Physics **100**, 074105 (2006); doi: 10.1063/1.2356905
View online: http://dx.doi.org/10.1063/1.2356905
View Table of Contents: http://scitation.aip.org/content/aip/journal/jap/100/7?ver=pdfcov
Published by the AIP Publishing

Electric-field-induced dielectric anomalies and optical birefringence in $Pb(Zn_{1/3}Nb_{2/3})_{1-x}Ti_xO_3$ ($x=0.10$) single crystal

C.-S. Tu[a] and F.-T. Wang
Graduate Institute of Applied Science and Engineering, Fu Jen University, Taipei 242, Taiwan

R. R. Chien and V. H. Schmidt
Department of Physics, Montana State University, Bozeman, Montana 59717

L.-C. Lim
Department of Mechanical Engineering, National University of Singapore, Singapore 119260, Singapore

(Received 12 May 2006; accepted 23 July 2006; published online 5 October 2006)

This work aims to study thermal stability, frequency response, and refractive indices in a (001)-cut $Pb(Zn_{1/3}Nb_{2/3})_{0.90}Ti_{0.10}O_3$ (PZNT10%) crystal before and after an electric (E)-field poling, which are important for piezoelectric and optical uses. Dielectric permittivities have been measured as functions of temperature, frequency, and poling strength. The dielectric absorption reveals a broad dipolar relaxation in the region of 260–310 K in the unpoled sample. Piezoelectric resonances were observed in the poled sample and show significant changes while phase transitions are taking place. The unpoled crystal shows almost no birefringence, indicating that the structure averaged over the optically anisotropic ferroelectric domains is optically isotropic. Birefringence appears after an E-field poling and shows a "negative" uniaxial distortion. The Cauchy equations for ordinary n_o and extraordinary n_e refractive indices were determined between 0.45 and 1.4 μm. However, the phase-matching criterion for second harmonic generation was not found. © *2006 American Institute of Physics*. [DOI: 10.1063/1.2356905]

I. INTRODUCTION

The relaxor-based ferroelectric (FE) crystals $Pb(Zn_{1/3}Nb_{2/3})_{1-x}Ti_xO_3$ (PZNT) have a morphotropic phase boundary (MPB) in the region of $\sim 5\% < x < \sim 14\%$ and exhibit successive phase transitions as temperature changes.[1] The spontaneous deformations of the tetragonal (T) state appear along the equivalent ⟨001⟩ directions, giving six FE domain states with optical axes oriented parallel to ⟨001⟩. In the low temperature region, the crystals exhibit rhombohedral (R) or orthorhombic (O) phases,[1,2] which have 8 equivalent R domain states along the ⟨111⟩ directions or 12 equivalent O domain states along the ⟨110⟩ directions. Large piezoelectric constants ($d_{33} \sim 1500 \times 10^{-12}$ C/N) and electromechanical coupling parameters ($k_{33} \sim 92\%$) have been reported in PZNT crystals.[3,4] Such high piezoelectricity has crucial applications in medical imaging and ultrasonic devices.

Piezoelectric resonance has been observed in poled $Pb(Zr_{1-x}Ti_x)O_3$ (PZT) ceramics[5] and piezoelectric polymers.[6] Multiple piezoelectric resonances were recently reported in $Pb(Mg_{1/3}Nb_{2/3})_{1-x}Ti_xO_3$ (PMNT) single crystals after a dc E-field poling and they occurred below 1.0 MHz.[7] It was found that the resonance spectra were sensitive to phase transformations and can be induced with a poling E-field less than the coercive field.[7] These dielectric resonances were found to be associated with vibrations of microscopic ionic units coupled to various extension modes. The frequency spectrum can be described by a damped-harmonic-oscillator model.[7]

Recently high-strain PMNT crystals have drawn attentions for optical applications, such as quasi-phase-matched second harmonic generation and electro-optic effects. Refractive indices of (001)-cut PMNT35% and 38% crystals show a clear birefringence after a prior poling, but the phase-matching condition was not satisfied.[7,8] The optical transmission was significantly enhanced by a prior E-field poling.[7,8] The refractive indices of unpoled PMNTx% crystals ($x=24$, 30, 31, and 33) increase with Ti content.[9]

To enhance piezoelectric performance, a prior E-field poling is usually done before these materials are employed in applications. However, how an E-field poling affects thermal stability and optical properties still remains unclear and is important for piezoelectric and optical uses. In this study, temperature- and frequency-dependent dielectric permittivities were investigated in a (001)-cut PZNT10% single crystal with and without a prior dc E-field poling. Optical transmission and refractive indices were also obtained as a function of wavelength.

II. EXPERIMENTAL PROCEDURE

The PZNT10% single crystal was grown using an improved flux growth method by Microfine Materials Technologies P/L, Singapore.[10] The sample was cut perpendicular to a ⟨001⟩ direction and its dimensions are $4.0 \times 2.0 \times 1.0$ mm^3. The Ti concentration (x%) was estimated by comparing the dielectric maximum temperature T_m (upon heating) with the phase diagram given in Ref. 1. A Wayne-Kerr precision analyzer PMA3260A was used to obtain real ε' and imaginary ε'' parts of dielectric permittivity. A Janis CCS-450 cold-head was used with a Lakeshore 340 control-

[a]Author to whom correspondence should be addressed; electronic mail: phys1008@mails.fju.edu.tw

ler. Gold electrodes were deposited on the (001) basal surfaces with an area of 4.0×2.0 mm^2 by dc sputtering. One basal surface of the sample was glued on a thin glass plate with silver paste for dielectric measurements. Three processes were used in the dielectric experiments. Two processes are called "zero-field-heated" (ZFH) and "zero-field-cooled" (ZFC), in which the data were taken upon heating and cooling, respectively, without any E-field poling. In another process, FR-ZFH, the sample was poled at room temperature (RT) with a dc E field applied along [001] for at least 1 h, followed by a ZFH measurement upward from 150 K. "FR" denotes that the poling was carried out at RT.

Frequency spectra of ε' and ε'' were carried out upon heating after poling at RT. A hysteresis loop was taken by using a Sawyer-Tower circuit at $f=46$ Hz. Refractive indices were measured at RT by using a Metricon model 2010 prism coupler equipped with three laser wavelengths, 0.473, 0.790, and 1.323 μm. Refractive index was determined by finding the critical angle of the total internal reflection and the polarization direction of the laser beam.

III. RESULTS AND DISCUSSION

Figures 1(a) and 1(b) show the temperature-dependent ε' and ε'' at several frequencies (0.5 kHz–1 MHz) obtained from ZFH, ZFC, FR-ZFH ($E=5$ kV/cm), and FR-ZFH ($E=8$ kV/cm), respectively. The frequency dispersions and thermal hystereses appear in the temperature regions of ~220–330 K and ~450–470 K, respectively, implying first-order transitions. ε' (FR-ZFH) splits into two frequency-dependent categories with an obvious gap. For $f\leqslant100$ kHz, the ε' (FR-ZFH: 5 kV/cm) shows successive anomalies near 300 and 340 K as indicated by the red and green arrows in Fig. 1(a). However, there is only a broad bump anomaly evidenced near 300 K in the ε' (FR–ZFH: 8 kV/cm) for $f\leqslant100$ kHz [Fig. 1(b)]. The dielectric maximum temperatures (T_m) of ε' (ZFH), ε' (FR-ZFH: 5 kV/cm), and ε' (FR-ZFH: 8 kV/cm) are respectively 467, 465, and 465 K, where the tetragonal-cubic ferroelectric transition occurs. The maximum values of ε' (FR-ZFH: 5 kV/cm) and ε' (FR-ZFH: 8 kV/cm), respectively, are $\sim3.4\times10^4$ and $\sim2.8\times10^4$ for $f=10$ kHz, which are smaller than the ε' (ZFH) by about 25% and 35%, respectively. This reduction is likely attributed to a smaller contribution of domain wall motion, because the E-field poling tends to remove such walls.

The dielectric absorptions ε'' (ZFH) and ε'' (ZFC) exhibit obvious frequency-dependent maxima in the region of 260–310 K, as shown in the insets of Fig. 1(a). This indicates that relaxation processes are involved in the dielectric thermal activities. Figure 2 shows a plot of frequency (f) vs $1000/T$. The temperatures (T) correspond to maxima of ε'' (ZFC) and ε'' (ZFH) for various frequencies in the region of 260–310 K. The phenomenological Vogel-Fulcher equation, $f=f_o\exp[-E_a/k_B(T-T_o)]$, is used to attain exponential fittings as expressed by solid lines. The fitting parameters are given in Fig. 2. f_o is a characteristic frequency (attempt frequency), E_a is the activation energy for orientation of electric dipoles, and T_o is the freezing temperature. What is the significance of these parameters? First, the attempt frequency is in the usual range for lattice vibrations. Second, T_o is the extrapolated temperature, below which all reorientation of clusters would cease according to this equation. However, a calculation based on the expansions in powers of $1/\ln(\tau\omega_o)$

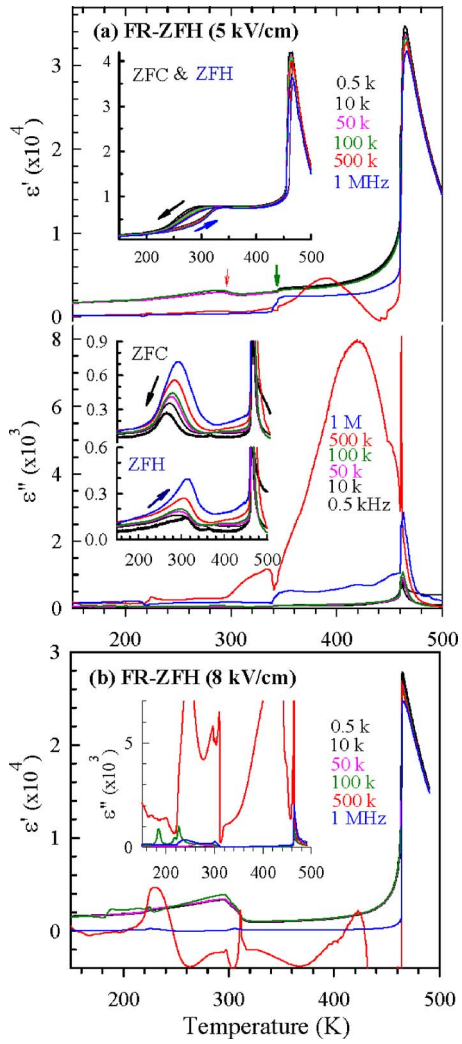

FIG. 1. (Color online) Dielectric permittivities (ε', ε'') of (a) ZFC, ZFH, and FR-ZFH (5.0 kV/cm) and (b) FR-ZFH (8.0 kV/cm).

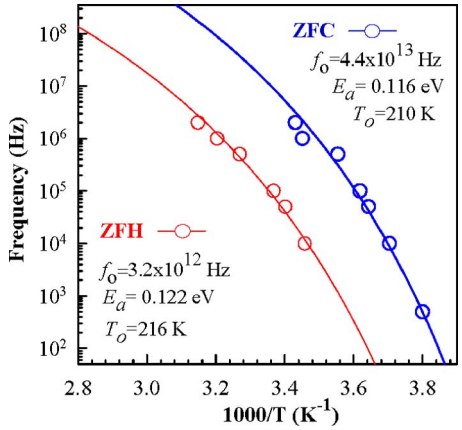

FIG. 2. (Color online) Plots of measured frequency (f) vs $1000/T$ for dispersions of ε'' in the range of 260–310 K. The solid curves are fittings of the Vogel-Fulcher equation with the parameters given in the figure.

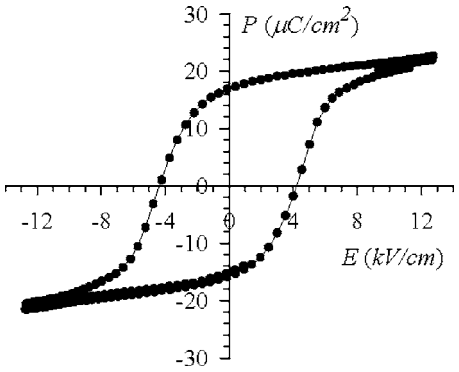

FIG. 3. Hysteresis loop of polarization vs E-field taken at RT.

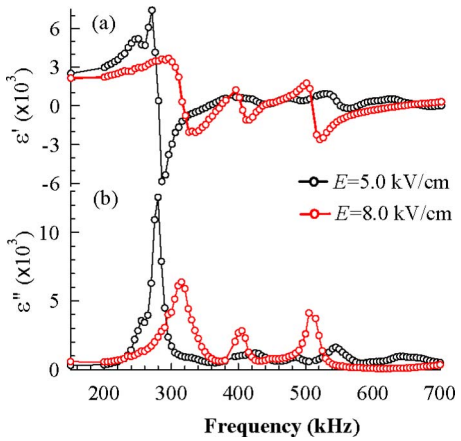

FIG. 4. (Color online) Frequency spectra of (a) ε' and (b) ε'' after poling with $E=5.0$ and 8.0 kV/cm at RT. The solid lines are guides for the eye. The sample thickness is 1.0 mm.

shows that an exponentially wide and smooth relaxation spectrum can also cause a Vogel-Fulcher behavior without manifest freezing (unlimited broadening of the relaxation time spectrum).[11] τ is relaxation time and ω_o is about $1/\tau_{\min}$. Third, E_a is the average of activation potential barriers for various clusters in this disordered system to reorient between adjacent variants. The slightly higher activation energy in ZFH implies a stronger correlation between polar clusters, which gives rise to a slower process to reach equilibrium in the system. Fitting the data to the Arrhenius law $[T_o=0]$ requires an unphysically high f_o. The use of the Vogel-Fulcher equation, which applies to disordered systems, is justified below T_C in the ferroelectric phase because this crystal is in the borderline region between ferroelectric and relaxor behaviors. The ferroelectric transition near 460 K appears nearly normal, but in addition to ferroelectric domains there are still some polar nanoclusters remaining below this transition that give rise to the Vogel-Fulcher behavior. The dynamics of polar nanoclusters has been considered to be responsible for the frequency-dependent relaxation behavior.[12] This interpretation is strengthened by the fact that this Vogel-Fulcher relaxation vanishes after poling at $E \geqslant 5$ kV/cm, because the polar nanoclusters then are incorporated into the ferroelectric domains or monodomain.

The ferroelectric hysteresis loop taken at RT and displayed in Fig. 3 sheds some light on whether the crystal is in a multidomain or in a monodomain state after the 5 kV/cm poling. The coercive field E_C and spontaneous polarization P_S are about 4.1 kV/cm and 18 μC/cm^2, respectively. The loop appears saturated at 5 kV/cm (above E_C) indicating a monodomain. However, our experience comparing polarizing microscopy pictures of domains with hysteresis loops taken on the same sample conditions indicates that apparent loop saturation may occur without all domains being incorporated into the majority domain.

After an E-field poling, both ε' and ε'' exhibit irregular resonant anomalies for $f>100$ kHz. These phenomena were not observed for poling fields $E \leqslant 3.0$ kV/cm, because this field is below E_C and so competing piezoelectric effects from different domains cancel. Figure 4 illustrates frequency spectra of ε' and ε'', in which multiple piezoelectric resonances occur between 0.1 and 0.7 MHz. The resonant frequencies are much smaller than the thickness extension mode of PZT ceramics.[5]

Figures 5(a) and 5(b) show temperature-dependent frequency spectra of ε'' after poling at $E=5.0$ and 8.0 kV/cm, respectively. The resonances mainly occur between 0.1 and 0.7 MHz. Below 300 K, as seen in Fig. 5(a) for $E=5$ kV/cm, the resonant spectra exhibit one main resonance near 300 kHz accompanied with two minor resonances at both sides. Resonance spectra exhibit an obvious change near 300 K, where minor resonances diminish. Note that a step-down dielectric anomaly was seen near 300 K in ε' (FR-ZFH: 5 kV/cm) for $f \leqslant 100$ kHz, as indicated by the red arrow in Fig. 1(a). The main resonance shifts to lower frequencies as temperature increases up to 340 K. The main resonance suddenly disappears above 340 K, which corresponds to a step-up anomaly in ε' (FR-ZFH: 5 kV/cm), as indicated by the green arrow in Fig. 1(a). With a stronger poling field of $E=8.0$ kV/cm, the frequency spectrum [Fig.

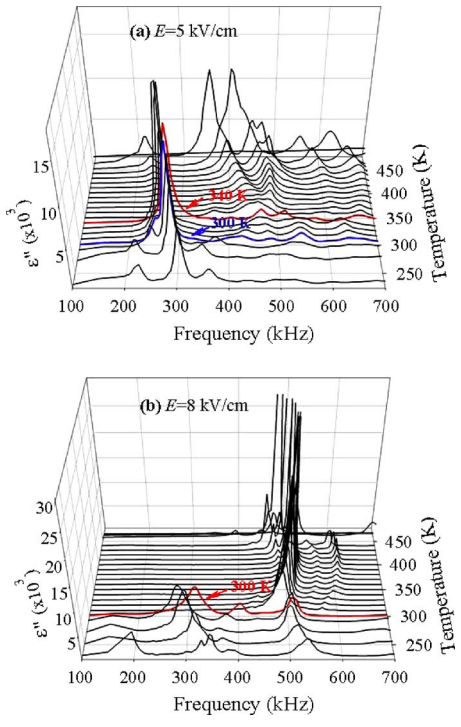

FIG. 5. (Color online) Temperature-dependent frequency spectra of ε'' after poling at (a) 5.0 and (b) 8.0 kV/cm.

5(b)] also exhibits multiple resonances below 300 K. The spectrum shows a significant transformation near 300 K, above which one sharp resonance comes into sight near 0.5 MHz. This is consistent with the anomaly seen near 300 K in the ε' (FR-ZFH: 8 kV/cm) for $f \leqslant 100$ kHz [Fig. 1(b)]. The appearance of the strong resonance near 0.5 MHz above 300 K implies a long-range ordered state.

What are the physical origins of these transformations near 300 and 340 K? An orthorhombic phase was found in PZNT9% and PZNT10% after an E-field poling.[2,13] Note that the poling E field in this study was along [001] which is a preferred polar direction for the tetragonal phase. From the phase diagram of PZNT crystals,[2,13] the poled (E=5.0 kV/cm) PZNT10% crystal likely undergoes an $O \rightarrow O(T) \rightarrow T \rightarrow C$ transition sequence near 300, 340, and 467 K upon heating. $O(T)$ represents that dominant O domains coexist with a smaller fraction of T domains. However, with a stronger poling field of E=8.0 kV/cm, the PZNT10% crystal likely undergoes an $O \rightarrow T \rightarrow C$ transition sequence with transitions near 300 and 467 K upon heating.

It was found that the resonant spectra can be described by the model of multiple forced-damped oscillators, i.e.,

$$\varepsilon(\omega)^* = \varepsilon'(\omega) - i\varepsilon''(\omega) = \varepsilon_c + \sum_{i=1} A_i \frac{(\omega_{oi}^2 - \omega^2) - i2\omega\gamma_i}{(\omega_{oi}^2 - \omega^2)^2 + 4\omega^2\gamma_i^2}, \quad (1)$$

where $\omega_{oi}(d)$ and $A_i(d)$ are the dimension-dependent resonant (or characteristic) frequency and amplitude for the ith oscillator. $\gamma_i(d)$ and ε_c are the damping factor and "clamped" dielectric permittivity, respectively. In this model, positive and negative ions are assumed to be placed at alternating layers. The applied ac electric field causes these ions to oscillate in opposite directions, as in a LO mode, but at much lower frequency than the natural frequency of the k=0 LO mode. When the crystal is in a piezoelectric (not cubic) phase, the $A_i(d)$ coefficients are nonzero and this field-excited LO motion is coupled to piezoelectric modes. The $\omega_{oi}(d)$ in Eq. (1) are the dimension-dependent natural frequencies of these piezoelectric modes. This dimensional dependence occurs because the piezoelectric resonance is a macroscopic cooperative phenomenon in which the sample size, shape, and boundary conditions play essential roles. To obtain Eq. (1), the ion motion was assumed to be like the one-dimensional forced-damped oscillation, i.e., $d^2z/dt^2 + 2\gamma(dz/dt) + \omega_o^2 z = (q/m)E_o\,\mathrm{Re}(e^{i\omega t})$, where $\gamma(d) = b(d)/2m$ and $\omega_o(d) = \sqrt{K(d)/m}$. $K(d)$, $b(d)$, and m are restoring-force constant, damping coefficient, and effective ion mass, respectively. The oscillating charges in PZNT can be the Pb^{+2} and $[(Zn_{1/3}Nb_{2/3})_{1-x}Ti_xO_3]^{-2}$ ionic sublattices. A similar mathematical analysis can be found in Ref. 5.

The dotted and solid lines in Fig. 6 illustrate fittings of Eq. (1) for resonant peaks (1 and 2) in the region of 200–350 kHz observed at RT after poling at E=5.0 kV/cm. The fitting parameters are given in Table I. The resonant frequencies of thickness and radial modes from the poled $Pb(Zr_{0.965}Ti_{0.035})O_3$ (PZT 96.5/3.5) ceramics were observed near 5.4 and 0.26 MHz, respectively.[5] The ratio of packed ion masses between $[(Zn_{1/3}Nb_{2/3})_{0.9}Ti_{0.1}O_3]^{-2}$ for PZNT and $[Zr_{0.965}Ti_{0.035}]O_3^{-2}$ for PZT 96.5/3.5 is about 0.93. Thus, peaks 1 and 2 in Fig. 6 most likely correspond to either width or length extension modes. The close frequencies between peaks 1 and 2 are likely due to crystal inhomogeneity. Manifold resonances are likely associated with spatial variation of Ti content and higher-order modes.

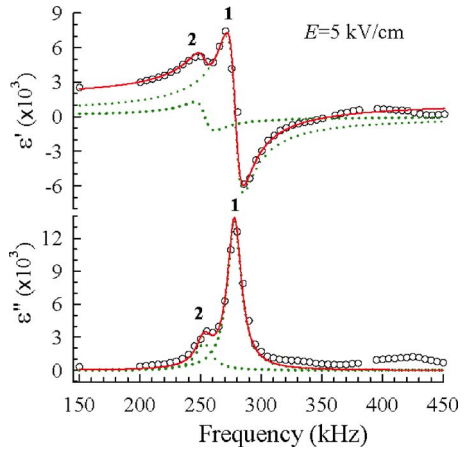

FIG. 6. (Color online) Frequency spectra of ε'' in the region of 150–450 kHz taken at 300 K for the sample poled at E=5.0 kV/cm. The dotted lines are fittings of Eq. (1) for peaks (1 and 2) with parameters in Table I. The solid line is the sum of fittings with ε_c=1200.

The piezoelectric resonant frequency depends on two parameters, namely, sample dimensions and sound velocity (which is a function of elastic stiffness and density). In general, the resonant frequency is proportional to the square root of the stiffness/density ratio and decreases with increasing sample dimension.[6] The detailed relations can be found in Ref. 6. In PZT ceramics, it was found that the characteristic frequency $\omega_o(d)$ is proportional to $1/d$ and can be written as $\omega_o(d) = \sqrt{K(2a)/m}(2a/d)$.[5] d can be thickness, width, or length of the sample. $K(2a)$ is the restoring-force constant with only two unit cells and a is the lattice parameter. In this study, the sample dimensions are $4.0 \times 2.0 \times 1.0$ mm^3. The major resonant frequencies at RT occur near 300 kHz, which likely correspond to width or length extension modes. Thus, we can estimate the ionic vibration frequency $\omega_o(2a)/2\pi$ by using the above equation and the sample's length (4.0 mm), i.e., $\omega_o(2a)/2\pi = \sqrt{K(2a)/m}/2\pi = [\omega_o(d)/2\pi](d/2a) \cong 1.5 \times 10^{12}$ Hz which is a reasonable value for an ionic vibration mode. Here, $\omega_o(d)/2\pi \cong 3.0 \times 10^5$ Hz and $a \cong 4.0$ Å are used.

Figure 7 shows ordinary n_o and extraordinary n_e refractive indices measured at RT for three laser wavelengths before and after a prior poling (E=8.0 kV/cm). In the poling process, the crystal was poled at RT along the [001] direction which is the optical axis of the uniaxial tetragonal structure. Both with and without a prior poling, the refractive indices

TABLE I. Fitting parameters of Eq. (1) in Fig. 6 with sample dimensions of $4.0 \times 2.0 \times 1.0$ mm^3.

Peak	$\omega_o/2\pi$ (kHz)	$A/(2\pi)^2$ (Hz^2)	$\gamma/2\pi$ (kHz)
1	278	5.3×10^{13}	7.0×10^3
2	253	1.0×10^{13}	8.0×10^3

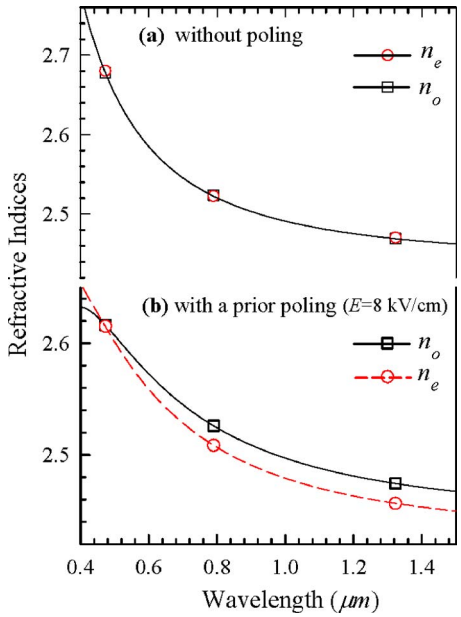

FIG. 7. (Color online) Refractive indices vs wavelength. The circle and square symbols represent the measured data from three wavelengths (0.473, 0.790, and 1.323 μm). The curves are the Cauchy fittings with parameters given in Table II.

n_e and n_o were measured for electric-field oscillation parallel to [001] and [010], respectively, for a laser beam propagating along [100]. The variation of refractive index measured from different spots on the sample surface is less than ±0.002. With a prior poling at E=8.0 kV/cm, the crystal exhibits negative birefringence. If we assume the crystal is poled into a single tetragonal domain, then this birefringence is uniaxial. Without prior poling, the crystal shows almost no birefringence, i.e., $|n_o - n_e| \cong 0$, indicating that the structural symmetry in PZNT10% averaged over the optically anisotropic ferroelectric domains is optically isotropic. One would expect the unpoled crystal to have numerous domains with random ferroelectric polarization directions that the light would propagate through, so that the apparent index of refraction n_a for the unpoled crystal would be $n_a=(2n_o+n_e)/3$ for uniaxial domains, where n_e and n_o now refer to the poled crystal. This relation is obeyed at the two longer wavelengths, but at 0.473 μm the unpoled crystal has about

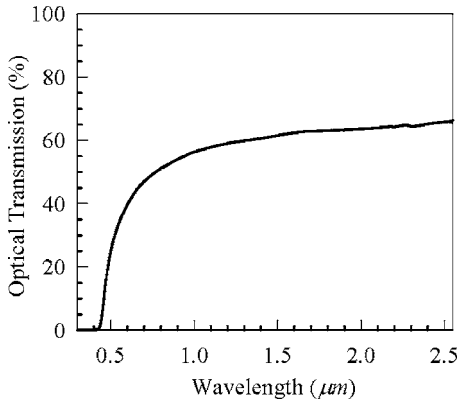

FIG. 8. Optical transmission vs wavelength. It was taken from the unpoled sample with 2.0 mm thickness.

TABLE II. The Cauchy equations for $n_o(\lambda)$ and $n_e(\lambda)$ obtained at RT for unpoled sample and sample with a prior poling (E=8.0 kV/cm), where λ is in microns.

1. E=0 (unpoled)	$n_o(\lambda) \cong n_e(\lambda) = 2.4400 + \frac{0.0506}{\lambda^2} + \frac{0.0006}{\lambda^4}$
2. E=8.0 kV/cm	$n_o(\lambda) = 2.4413 + \frac{0.0606}{\lambda^2} + \frac{-0.0048}{\lambda^4}$
	$n_e(\lambda) = 2.4246 + \frac{0.0578}{\lambda^2} + \frac{-0.0034}{\lambda^4}$

0.06 greater index than the poled crystal. This difference is barely outside experimental error. Note from the previous discussion that the unpoled crystal may have some orthorhombic domains and nanopolar regions as well as tetragonal domains, which could account for any difference in index from the above average-value expression. The birefringence $|n_o - n_e|$ for the poled crystal is about 0.0176 at $\lambda = 0.790$ μm, which is larger than 0.0129 obtained from a (001)-cut poled PMNT35% crystal.[14] By fitting refractive indices, the Cauchy equations for n_o and n_e were acquired for both unpoled and poled samples, as given in Table II. The overall refractive indices are smaller than the (001)-cut PMNT35% crystal.[14] The phase-matching angle[15] for the second harmonic generation is not found in this study.

Wavelength-dependent optical transmission from 0.3 to 2.5 μm given in Fig. 8 shows no absorption before reaching the cutoff wavelength $\lambda \cong 0.4$ μm, which is the same with and without a prior poling. The transmission cutoff at $\lambda \cong 0.4$ μm implies a low-lying electronic energy gap ($E_g \cong hc/\lambda$) of ~3.0 eV. The transmission of PMNT crystals also goes to zero at $\lambda \cong 0.4$ μm.[14]

IV. CONCLUSIONS

This work has revealed dipolar relaxation behavior in the region of 260–310 K in the unpoled (001)-cut PZNT10% crystal, and evidence of piezoelectric resonances after a prior poling for $E \geqslant 5.0$ kV/cm. The field-induced dielectric/piezoelectric resonances mostly occur in the region of 0.1–0.7 MHz and disappear as temperature approaches T_m. The resonant spectrum is sensitive to microscopic structure dynamics, and is a valuable characterization method to study phase transformations. The unpoled PZNT10% shows no optical birefringence as expected, but significant birefringence was attained by a prior E-field poling. The Cauchy equations of refractive indices n_o and n_e were obtained, but the phase-matching condition for second harmonic generation was not found. Higher poling field may be needed to completely pole the crystal and thus enhance birefringence.

ACKNOWLEDGMENTS

This work was supported by National Science Council (NSC) of Taiwan Grant No. 94-2112-M-030-004.

[1] J. Kuwata, K. Uchino, and S. Nomura, Ferroelectrics **37**, 579 (1981).
[2] D. E. Cox, B. Noheda, G. Shirane, Y. Uesu, K. Fujishiro, and Y. Yamada, Appl. Phys. Lett. **79**, 400 (2001).
[3] Y. Yamashita, Jpn. J. Appl. Phys., Part 1 **33**, 5328 (1994).
[4] R. F. Service, Science **275**, 1878 (1997).

[5]N. Cereceda, B. Noheda, J. R. Fdez.-del-Castillo, J. A. Gonzalo, J. De Frutos, and A. M. González, J. Eur. Ceram. Soc. **19**, 1259 (1999).
[6]A. Mellinger, IEEE Trans. Dielectr. Electr. Insul. **10**, 842 (2003).
[7]C.-S. Tu, R. R. Chien, V. H. Schmidt, F. T. Wang, W. T. Hsu, C. T. Tseng, and C. C. Shih, J. Appl. Phys. **97**, 126105 (2005).
[8]X. Wan, H. Xu, T. He, D. Lin, and H. Luo, J. Appl. Phys. **93**, 4766 (2003).
[9]X. Wan, H. L. W. Chan, C. L. Choy, Z. Zhao, and H. Luo, J. Appl. Phys. **96**, 1387 (2004).
[10]L. C. Lim and K. K. Rajan, J. Cryst. Growth **271**, 435 (2004).
[11]A. K. Tagantsev, Phys. Rev. Lett. **72**, 1100 (1994).
[12]D. Viehland, S. J. Jang, L. E. Cross, and M. Wuttig, Phys. Rev. B **46**, 8003 (1992).
[13]D. La-Orauttapong, B. Noheda, Z. G. Ye, P. M. Gehring, J. Toulouse, D. E. Cox, and G. Shirane, Phys. Rev. B **65**, 144101 (2002).
[14]C.-S. Tu, F.-T. Wang, R. R. Chien, V. H. Schmidt, and G. F. Tuthill, J. Appl. Phys. **97**, 064112 (2005).
[15]A. Yariv, *Optical Electronics* (Saunders College Publishing, San Francisco, CA, 1991), pp. 270–274.